

SPECTROSCOPIC CONFIRMATION OF A MASSIVE RED-SEQUENCE SELECTED GALAXY CLUSTER AT $Z = 1.34$ IN THE SPARCS-SOUTH CLUSTER SURVEY

GILLIAN WILSON¹, ADAM MUZZIN², H. K. C. YEE³, MARK LACY⁴, JASON SURACE⁴, DAVID GILBANK⁵, KRIS BLINDERT⁶, HENK HOEKSTRA^{7,8,9}, SUBHABRATA MAJUMDAR¹⁰, RICARDO DEMARCO¹, JONATHAN P. GARDNER¹¹, MICHAEL D. GLADDERS¹², AND CAROL LONSDALE^{13,14}

Draft version October 25, 2018

ABSTRACT

The Spitzer Adaptation of the Red-sequence Cluster Survey (SpARCS) is a z' -passband imaging survey, consisting of deep ($z' \simeq 24$ AB) observations made from both hemispheres using the CFHT 3.6m and CTIO 4m telescopes. The survey was designed with the primary aim of detecting galaxy clusters at $z > 1$. In tandem with pre-existing $3.6\mu\text{m}$ observations from the *Spitzer* Space Telescope SWIRE Legacy Survey, SpARCS detects clusters using an infrared adaptation of the two-filter red-sequence cluster technique. The total effective area of the SpARCS cluster survey is 41.9 deg^2 . In this paper, we provide an overview of the 13.6 deg^2 Southern CTIO/MOSAICII observations. The 28.3 deg^2 Northern CFHT/MegaCam observations are summarized in a companion paper by Muzzin et al. (2008a). In this paper, we also report spectroscopic confirmation of SpARCS J003550-431224, a very rich galaxy cluster at $z = 1.335$, discovered in the ELAIS-S1 field. To date, this is the highest spectroscopically confirmed redshift for a galaxy cluster discovered using the red-sequence technique. Based on nine confirmed members, SpARCS J003550-431224 has a preliminary velocity dispersion of $1050 \pm 230 \text{ km s}^{-1}$. With its proven capability for efficient cluster detection, SpARCS is a demonstration that we have entered an era of large, homogeneously-selected $z > 1$ cluster surveys.

Subject headings: surveys — cosmology: observations — galaxies: clusters: general — galaxies: high-redshift — infrared: galaxies

1. INTRODUCTION

Dating back to the pioneering photographic work of the mid-twentieth century (Abell 1958; Zwicky et al. 1968), galaxy cluster surveys have held a special place in the history of Astronomy. Due to the limitations of photographic plates, however, early optical surveys struggled to discover clusters at redshifts higher than $z \simeq 0.2$.

Galaxy cluster surveys were revolutionized by the launch of a series of powerful X-ray observatories in the

1980's and 1990's. Firstly *Einstein*, then *ROSAT*, and later the XMM and *Chandra* telescopes proved their capability to detect clusters out to $z = 1$. For example, the wide but relatively shallow 734 deg^2 *Einstein* Medium-Sensitivity Survey (Gioia et al. 1990, EMSS) both provided the base catalog for the Canadian Network for Observation Cosmology (CNOC1) survey of clusters at $z \sim 0.4$ (Yee et al. 1996), and discovered MS 1054-03 at $z = 0.83$ (Gioia & Luppino 1994), a massive cluster which provided the first evidence that Ω_m was significantly < 1 (Donahue et al. 1998). The deeper but smaller 48 deg^2 *ROSAT* Deep Cluster Survey (Rosati et al. 1998, RDCS) detected RX J0848.9+4452 at $z = 1.26$, which was, at the time, one of the most distant clusters to be discovered (Rosati et al. 1999).

The advent of large-format charge coupled devices (CCDs) brought renewed interest in carrying out optical cluster surveys e.g., the 6 deg^2 Palomar Distant Cluster Survey (Postman et al. 1996, PDCS), the 16 deg^2 KPNO survey of Postman et al. (1998), and the 135 deg^2 Las Campanas Distant Cluster Survey (Gonzalez et al. 2001, LCDCS) from which the ESO Distant Cluster Survey (White et al. 2005, EDisCS) was selected. All three of these surveys used variants of the matched-filter method to detect clusters.

In an effort to combat “false positive” detections caused by line-of-sight projections of unrelated systems in single-passband optical cluster searches, Gladders & Yee (2000) proposed a two-filter technique. Their Cluster Red-Sequence (CRS) technique was motivated by the observational fact that galaxy clusters contain a population of early-type galaxies which follow a tight color-magnitude relation. This relation has

¹ Department of Physics and Astronomy, University of California, Riverside, CA 92521; gillianw@ucr.edu

² Department of Astronomy, Yale University, New Haven, CT, 06520-8101

³ Department of Astronomy and Astrophysics, University of Toronto, 50 St. George St., Toronto, Ontario, Canada, M5S 3H4

⁴ Spitzer Science Center, California Institute of Technology, 220-6, Pasadena, CA 91125

⁵ Astrophysics and Gravitation Group, Department of Physics and Astronomy, University Of Waterloo, Waterloo, Ontario, Canada, N2L 3G1

⁶ Max Planck Institute for Astronomy Koenigstuhl 17, 69117, Heidelberg, Germany

⁷ Department of Physics and Astronomy, University of Victoria, Victoria, BC V8P 5C2, Canada

⁸ Leiden Observatory, Leiden University, PO Box 9513, 2300RA Leiden, The Netherlands

⁹ Alfred P. Sloan Fellow

¹⁰ Department of Astronomy and Astrophysics, Tata Institute of Fundamental Research (TIFR), Homi Bhabha Road, Mumbai, India

¹¹ Goddard Space Flight Center, Code 665, Laboratory for Observational Cosmology, Greenbelt MD 20771

¹² Department of Astronomy and Astrophysics, University of Chicago, 5640 South Ellis Avenue, Chicago, IL 60637

¹³ Infrared Processing and Analysis Center, California Institute of Technology, 220-6, Pasadena, CA 91125

¹⁴ North American ALMA Science Center, NRAO Headquarters, 520 Edgemont Road, Charlottesville, VA 22903

been shown to have an extremely small scatter (e.g., Bower et al. 1992), even to redshifts as high as $z \sim 1.4$ (Blakeslee et al. 2003; Holden et al. 2004; Lidman et al. 2008). If two filters which bracket the 4000\AA break are used to construct color-magnitude diagrams, early types are always the brightest, reddest galaxies at any redshift, and provide significant contrast from the field. The CRS method has been used for the $\sim 100 \text{ deg}^2$ Red-sequence Cluster Survey (RCS-1, Gladders & Yee 2005) and is also being used for the next generation $\sim 1000 \text{ deg}^2$ RCS-2 survey (Yee et al. 2007). Both of these surveys use an $R - z'$ filter combination. A variant of the red sequence method (the BCGmax algorithm) has also been used to detect clusters in the Sloan Digital Sky Survey (Koester et al. 2007a,b). In addition to detecting clusters with a very low false-positive rate, a second important advantage of the CRS technique is that it also provides a good photometric estimate of the cluster redshift, accurate to $\Delta z \sim 0.05$ at $z < 1$ (Gilbank et al. 2007).

Applying the CRS technique to searching for clusters at higher redshift was an obvious next step which was not feasible until very recently, because of technical limitations. At $z \sim 1.2$, the z' filter is no longer redward of the rest-frame 4000\AA break, requiring the use of large-format near-infrared cameras which have only recently begun to appear on 4m telescopes (Dalton et al. 2006; Warren et al. 2007). Another issue is that the sky itself is bright in the infrared, requiring longer integration times than for optical imaging.

The first real opportunity to systematically detect galaxy clusters at $z > 1$ in large numbers was presented in 2003 with the launch of the InfraRed Array Camera (IRAC; Fazio et al. 2004) onboard the *Spitzer* Space Telescope (Werner et al. 2004). Both our own pilot study carried out using the 3.8 deg^2 60s-depth First Look Survey (FLS Lacy et al. 2005; Wilson et al. 2005; Muzzin et al. 2008b), and that carried out using the 8.5 deg^2 90s-depth IRAC Shallow Survey (Eisenhardt et al. 2004; Stanford et al. 2005; Brodwin et al. 2006; Eisenhardt et al. 2008), quickly demonstrated the power of IRAC for $z > 1$ cluster detection.

Clusters of galaxies are extremely rare and one requires a widefield survey to find the most massive examples. The largest area *Spitzer* Space Telescope Survey is the 50 deg^2 120s-depth SWIRE Legacy Survey (Lonsdale et al. 2003). In § 2, we provide an overview of SpARCS¹⁵, our z' -imaging survey of the six SWIRE fields. We also summarize the Southern observations. In § 3, we briefly review our red-sequence detection algorithm and introduce a rich cluster candidate selected in the CTIO ELAIS-S1 field. We present Gemini/GMOS-S spectroscopic follow-up of SpARCS J003550-431224 in § 4, confirming it to be, at $z = 1.34$, the highest redshift cluster yet discovered using the red-sequence technique. We discuss our main results in § 5 and conclude in § 6. We assume an $\Omega_{m0} = 0.3, \Omega_{\lambda0} = 0.7$ cosmology with $H_0 = 70 \text{ km s}^{-1} \text{ Mpc}^{-1}$ throughout.

2. SPARCS SURVEY IMAGING

2.1. Choice of Passbands

The *Spitzer* SWIRE Legacy Survey is a seven pass-band imaging survey consisting of IRAC 3.6, 4.5, 5.8, 8.0 μm and Multiband Imaging Photometer for *Spitzer* (MIPS; Rieke et al. 2004) 24, 70, 160 μm observations. Full details of the survey design, data processing, ancillary datasets and source catalogs may be found in Surace et al. (2005). For cluster detection SpARCS utilizes $3.6\mu\text{m}$, the most sensitive *Spitzer* channel, as its “red” filter.

SpARCS utilizes z' as its “blue” filter. Simulations (e.g., see Wilson et al. 2006) showed a limiting magnitude of $z \sim 24$ AB was required to match the $3.6\mu\text{m}$ depth. It was necessary to obtain our own widefield z' -imaging for only five of the six SWIRE fields (Table 1), because observations of the XMM-LSS field were available from the Canada-France-Hawaii Telescope (CFHT) Legacy Survey¹⁶. Those observations were made either using the MOSAICII instrument on the 4m Blanco telescope at the Cerro Tololo Inter-American Observatory (CTIO) in the case of the Southern fields (ELAIS-S1 and Chandra-S) or using MegaCam at the 3.6m CFHT in the case of the Northern fields (ELAIS-N1, ELAIS-N2 and Lockman). A summary of the latter observations, and spectroscopic confirmation of two clusters at $z = 1.18$ and $z = 1.20$ in the ELAIS-N2 field may be found in the companion paper by Muzzin et al. (2008a).

2.2. The CTIO Dataset

The SWIRE IRAC $3.6\mu\text{m}$ Southern fields are shown in Figure 1. The $3.6\mu\text{m}$ mosaic of the ELAIS-S1 field totals 7.1 deg^2 and the Chandra-S field totals 8.1 deg^2 (see Table 1)

The 8192×8192 pixel MOSAIC II camera on the 4m Blanco telescope has a pixel scale of $0.''267 \text{ pixel}^{-1}$, leading to a $36' \times 36'$ footprint per pointing. The white squares overlaid on Figure 1 show the 46 CTIO MOSAICII pointings required to image the ELAIS-S1 and Chandra-S fields. These pointings were designed to maximize the overlap with the $3.6\mu\text{m}$ data, but to minimize the overall number of pointings by omitting regions with little overlap with the IRAC data. The total area of the z' observations per field is shown in Table 1.

CTIO observations were made of the ELAIS-S1 and Chandra-S fields using the z' filter on a total of 17 nights. The depth of the z' data varies from pointing to pointing depending on the seeing and the sky background; however, the mean depth is 24.0 AB (23.5 Vega; 5σ). Table 1 shows the total effective area per field, i.e., the total usable area of overlap between the z' and $3.6\mu\text{m}$ datasets once areas of bright star contamination and chips gaps have been excluded. The total effective area of the CTIO fields is 13.6 deg^2 (6.5 deg^2 in the ELAIS-S1 and 7.1 deg^2 in the Chandra-S fields), and the total effective area of the six fields is 41.9 deg^2 .

3. CLUSTER DETECTION

We defer a full description of the SpARCS data reduction, cluster candidate detection algorithm and catalogs to Muzzin et al. 2009, in prep. However, we note that the algorithm used here is almost identical to that described in Muzzin et al. (2008b), as applied to the *Spitzer*

¹⁵ <http://www.faculty.ucr.edu/~gillianw/SpARCS>

¹⁶ <http://www.cfht.hawaii.edu/Science/CFHTLS/>

First Look Survey (FLS; Lacy et al. 2005; Wilson et al. 2005). The one important difference is that Muzzin et al. (2008b) used an $R - [3.6]$ color to detect clusters at $0 < z < 1.3$ in the FLS. The slightly deeper SWIRE exposure time, combined with the $z' - [3.6]$ color choice, allows SpARCS to detect clusters to higher redshift than possible with the FLS dataset.

3.1. SpARCS J003550-431224

From analysis of the ELAIS-S1 field, SpARCS J003550-431224, shown in Figure 2, was identified as a high probability rich cluster candidate. SpARCS J003550-431224 (R.A.: 00:35:49.7, Dec.: -43:12:24.16) has a $B_{gc,R}$ ¹⁷ richness of $1055 \pm 276 \text{ Mpc}^{1.8}$ (for a discussion of B_{gc} and $B_{gc,R}$ see Yee & López-Cruz 1999 and Gladders & Yee 2005). Based on the empirical calibration of B_{gc} vs. M_{200} determined by Muzzin et al. (2007) in the K-band for the CNOC1 clusters at $z \sim 0.3$, this implies $M_{200} = 5.7 \times 10^{14} M_{\odot}$.

4. SPECTROSCOPY

Spectroscopic follow-up of SpARCS J003550-431224 was obtained with the Gemini Multi-Object Spectrograph on the Gemini South telescope (GMOS-S) in queue mode (program ID GN-2007B-Q16). We used $1.0''$ wide slits. We used GMOS with the R150 grism, blazed at 7170Å . This provided a spectral resolving power of $R = 631$ which corresponds to a resolution of 11Å , or 280 km s^{-1} at the redshift of the cluster.

We observed a single mask for 10 hrs. The mask was observed using the OG515 filter which blocks light blueward of 5150Å . The central wavelength of the grating was moved between 7380Å , 7500Å , and 7620Å to “dither” in the dispersion direction and fill in GMOS chip gaps. We used nod-&-shuffle in band-shuffle mode. This is slightly less efficient than micro-shuffle mode but allows one to maximize the number of slits in a small area, such as is the case for a distant cluster with a high surface density of red-sequence galaxies concentrated in the cluster core (see Figure 2). There were 26 slits on the mask, including three alignment stars. Slits were placed on galaxies with priorities from 1 to 5. Priority 1 (single digit ID #'s in Table 2) was galaxies with colors within 0.6 magnitude of the red sequence, and with $[3.6] < 17.0$ (Vega). Priority 2 (ID #'s in the 1000's) was galaxies with colors within 0.6 magnitude of the red sequence, and with $17.0 < [3.6] < 18.0$. Priority 3 (ID #'s in the 2000's) was galaxies with colors bluer than the red sequence by 0.6 – 1.0 magnitude, and with $[3.6] < 17.5$. Priority 4 (ID #'s in the 3000's) was galaxies with colors bluer than the red-sequence by 1.0 – 1.5 magnitude, and with $[3.6] < 17.5$. Priority 5 (ID #'s in the 4000's) was the lowest priority and included all galaxies with magnitude $16.9 < [3.6] < 18.0$. Priorities 1 to 4 roughly correspond to bright red-sequence, faint red-sequence, blue cloud, and extreme blue cloud galaxies respectively. Each exposure was 30 minutes in duration. The 20 exposures used nod cycles of 60s integration time per cycle and were offset by a few arcseconds using the on-chip dithering option.

¹⁷ We use the $z' - [3.6]$ vs. $3.6\mu\text{m}$ red-sequence to determine $B_{gc,R}$.

4.1. Data Reduction

The data were reduced using standard GeminiIRAF routines to bias-subtract the data. The iGDDS package (Abraham et al. 2004) was used to interactively trace the 2D spectra and extract 1D spectra. Wavelength-calibration for each extracted spectrum was performed using bright sky lines from the unsubtracted image, also with the iGDDS software. Wavelength solutions typically have an r.m.s. $< 0.5\text{Å}$. We determined a relative flux calibration curve using a long slit observation of the standard star EG21. We determined redshifts by identifying prominent spectra features such as Calcium H+K lines at 3934Å and 3968Å and the [OII] $\lambda\lambda 3727$ doublet using the iGDDS code. A few of the spectra also show some Balmer series lines.

Spectra were obtained for 15 of the 23 photometrically selected galaxies with quality sufficient for determining redshifts: the other eight were deemed too faint for reliable identification of spectral features. Table 2 shows ten galaxies, which were deemed likely to be cluster members based upon the value of their spectroscopic redshifts (although see § 5). These galaxies are indicated by white boxes in the right panel of Figure 2. Some examples of the spectra of confirmed members are shown in Figure 3. These spectra have been smoothed by a 7-pixel boxcar (which produces a resolution equal to that of the spectrograph).

A total of five galaxies were determined to be foreground or background sources. These galaxies are also listed in Table 2 and indicated by green boxes in the right panel of Figure 2. The histogram in the left panel of Figure 4 shows the spectroscopic redshifts of all 15 galaxies. The histogram in the right panel shows only the redshifts of the 10 likely cluster members.

5. DISCUSSION

Before calculating a redshift and velocity dispersion for SpARCS J003550-431224, we first checked for near-field interlopers using the code of Blindert (2006). This employs a modified version of the Fadda et al. (1996) shifting-gap technique, and uses both galaxy position and velocity information. Figure 5 shows galaxy velocities relative to the mean velocity, as a function of radius. The galaxy marked with an “x” (ID 5 at $z = 1.315$ in Table 2) was identified as being more likely to be a near-field object than a member of the cluster and was not used in the computation of the velocity dispersion or the mean redshift of the cluster. (This is also the lowest redshift galaxy in the right panel of Figure 4). A mean redshift of $z = 1.335$ and a velocity dispersion of $1050 \pm 230 \text{ km s}^{-1}$ was calculated for SpARCS J003550-431224. The uncertainty on the latter was determined using Jackknife resampling of the data.

It is, as yet, unclear as to whether SpARCS J003550-431224 is a relaxed cluster or a system in the process of collapsing. The distribution in Figure 4 (right panel) appears non-Gaussian and there is some evidence of bimodality. For comparison, a Gaussian with an r.m.s. of 1050 km s^{-1} has been overlaid on the right panel of Figure 4. The velocity dispersion of $1050 \pm 230 \text{ km s}^{-1}$ should certainly be considered “preliminary”, based, as it is, upon only nine members. However, if one does adopt this value of velocity dispersion, one can use it to cal-

culate a dynamical estimate of r_{200} (the radius at which the mean interior density is 200 times the critical density, ρ_c) using the equation of Carlberg et al. (1997):

$$r_{200} = \frac{\sqrt{3}\sigma}{10H(z)}, \quad (1)$$

where $H(z)$ is the Hubble parameter at the redshift of the cluster. This gives a value of $r_{200} = 1.2 \pm 0.3$ Mpc. From this, the dynamical mass M_{200} , the mass contained within r_{200} , can also be inferred using:

$$M_{200} = \frac{4}{3}\pi r_{200}^3 \cdot 200\rho_c, \quad (2)$$

We estimate a dynamical mass of $M_{200} = (9.4 \pm 6.2) \times 10^{14} M_\odot$ for J003550-431224, which is in good agreement with, albeit slightly larger than, the value of $M_{200} = 5.7 \times 10^{14} M_\odot$, which was calculated based upon its richness. Further spectroscopy is certainly warranted, but the preliminary evidence suggests that SpARCS J003550-431224 is a massive cluster, perhaps the most massive cluster at $z > 1$ in our 42 deg² survey.

The color-magnitude diagram for all galaxies in a 550 kpc (65'') radius of the cluster center is shown in Figure 6. The red diamonds show the 10 cluster members from Table 2. The blue diamonds show the two (of five) confirmed foreground/background galaxies that fall within the 550 kpc radius.

Based on its red-sequence color of $z' - [3.6] = 5.4$ (shown as dotted line in Figure 6), SpARCS J003550-431224 was originally assigned a photometric redshift of $z = 1.57$. This was based on Bruzual & Charlot (2003, BC03) models assuming a formation redshift $z_f = 4$. If one assumes a formation redshift of $z_f = 10$, then the $z' - [3.6] = 5.4$ color would cause one to infer a photometric redshift of $z = 1.39$ for SpARCS J003550-431224, which is reasonably consistent with the spectroscopic value. One possibility for the overestimate of the photometric redshift is that the BC03 models are too blue at young ages, as suggested by Maraston (2005). Spectroscopy of additional $z \sim 1.35$ SpARCS clusters will determine whether SpARCS J003550-431224's red-sequence color is representative for this redshift, or if there is something atypical about this particular cluster.

6. CONCLUSIONS

In this paper, we reported the discovery of SpARCS J003550-431224 in the ELAIS-S1 field, a very rich galaxy cluster at $z = 1.335$, with a preliminary velocity dispersion of 1050 ± 230 km s⁻¹. Several other rich $z > 1$ clusters in the SpARCS survey have also been spectroscopically confirmed (Muzzin et al. 2008a, Demarco et al. 2008, in prep), with no false positives.

The FLS, IRAC Shallow Cluster Survey (ISCS) and SpARCS have demonstrated the power and potential of widefield infrared observations from space for $z > 1$ cluster surveys. Both the FLS and SpARCS surveys are very similar to the RCS-1 and RSC-2 surveys, except that they utilize an optical-infrared adaptation of the CRS technique (the ISCS uses a multipassband photometric technique). SpARCS, in particular, is a demonstration that $z > 1$ cluster detection is now routine. With its two filter red-sequence detection algorithm, it is both highly

efficient and robust against line-of-sight projections. At 42 deg², the SpARCS cluster survey is also currently the only $z > 1$ survey sufficiently large to select clusters *both* as a function of redshift and richness.

It is noteworthy that all the $z > 1$ SpARCS clusters were discovered in only 120s per pointing of IRAC observations. Since clusters are rare, widefield cluster searches are required to discover the most massive examples. To discover a representative sample of massive structures at $z > 1.5$ would require an even wider survey, of several hundred square degrees, a proposition which would be feasible during the lifetime of the *Spitzer* Space Telescope Warm Mission (Gardner et al. 2007; Stauffer et al. 2007).

The authors wish to thank the staff of The Cerro Tololo Inter-American Observatory for their invaluable assistance, without which this work would not have been possible. CTIO is operated by the Association of Universities for Research in Astronomy, under contract with the National Science Foundation.

Based on observations obtained at the Gemini Observatory, which is operated by the Association of Universities for Research in Astronomy, Inc., under a cooperative agreement with the NSF on behalf of the Gemini partnership: the National Science Foundation (United States), the Science and Technology Facilities Council (United Kingdom), the National Research Council (Canada), CONICYT (Chile), the Australian Research Council (Australia), Ministerio da Ciencia e Tecnologia (Brazil) and SECYT (Argentina)

This work is based in part on archival data obtained with the Spitzer Space Telescope, which is operated by the Jet Propulsion Laboratory, California Institute of Technology under a contract with NASA. Support for this work was provided by an award issued by JPL/Caltech. GW acknowledges support from the College of Natural and Agricultural Sciences at UCR.

REFERENCES

- Abell, G. O. 1958, *ApJS*, 3, 211
- Abraham, R. G., et al. 2004, *AJ*, 127, 2455
- Blakeslee, J. P., et al. 2003, *ApJ*, 596, L143
- Blindert, K. 2006, Ph.D. thesis, University of Toronto (Canada)
- Bower, R. G., Lucey, J. R., & Ellis, R. S. 1992, *MNRAS*, 254, 601
- Brodwin, M., et al. 2006, *ApJ*, 651, 791
- Bruzual, G., & Charlot, S. 2003, *MNRAS*, 344, 1000
- Carlberg, R. G., et al. 1997, *ApJ*, 485, L13
- Dalton, G. B., et al. 2006, in *Society of Photo-Optical Instrumentation Engineers (SPIE) Conference Series*, Vol. 6269, Society of Photo-Optical Instrumentation Engineers (SPIE) Conference Series
- Donahue, M., Voit, G. M., Gioia, I., Lupino, G., Hughes, J. P., & Stocke, J. T. 1998, *ApJ*, 502, 550
- Eisenhardt, P. R., et al. 2004, *ApJS*, 154, 48
- Eisenhardt, P. R. M., et al. 2008, *ApJ*, 684, 905
- Fadda, D., Girardi, M., Giuricin, G., Mardirossian, F., & Mezzetti, M. 1996, *ApJ*, 473, 670
- Fazio, G. G., et al. 2004, *ApJS*, 154, 10
- Gardner, J. P., Fan, X., Wilson, G., & Stiavelli, M. 2007, in *American Institute of Physics Conference Series*, Vol. 943, The Science Opportunities of the Warm Spitzer Mission Workshop, ed. L. J. Storrie-Lombardi & N. A. Silbermann, 229
- Gilbank, D. G., Yee, H. K. C., Ellingson, E., Gladders, M. D., Barrientos, L. F., & Blindert, K. 2007, *AJ*, 134, 282
- Gioia, I. M., Henry, J. P., Maccacaro, T., Morris, S. L., Stocke, J. T., & Wolter, A. 1990, *ApJ*, 356, L35
- Gioia, I. M., & Luppino, G. A. 1994, *ApJS*, 94, 583
- Gladders, M. D., & Yee, H. K. C. 2000, *AJ*, 120, 2148
- Gladders, M. D., & Yee, H. K. C. 2005, *ApJS*, 157, 1
- Gonzalez, A. H., Zaritsky, D., Dalcanton, J. J., & Nelson, A. 2001, *ApJS*, 137, 117
- Holden, B. P., Stanford, S. A., Eisenhardt, P., & Dickinson, M. 2004, *AJ*, 127, 2484
- Koester, B. P., et al. 2007a, *ApJ*, 660, 239
- Koester, B. P., et al. 2007b, *ApJ*, 660, 221
- Lacy, M., et al. 2005, *ApJS*, 161, 41
- Lidman, C., et al. 2008, *ArXiv e-prints*
- Lonsdale, C. J., et al. 2003, *PASP*, 115, 897
- Maraston, C. 2005, *MNRAS*, 362, 799
- Muzzin, A., et al. 2008a, (*astro-ph/0810.0005*)
- Muzzin, A., Wilson, G., Lacy, M., Yee, H. K. C., & A, S. S. 2008b, in press, (*astro-ph/0807.0227*)
- Muzzin, A., Yee, H. K. C., Hall, P. B., & Lin, H. 2007, *ApJ*, 663, 150
- Postman, M., Lauer, T. R., Szapudi, I., & Oegerle, W. 1998, *ApJ*, 506, 33
- Postman, M., Lubin, L. M., Gunn, J. E., Oke, J. B., Hoessel, J. G., Schneider, D. P., & Christensen, J. A. 1996, *AJ*, 111, 615
- Rieke, G. H., et al. 2004, *ApJS*, 154, 25
- Rosati, P., della Ceca, R., Norman, C., & Giacconi, R. 1998, *ApJ*, 492, L21
- Rosati, P., Stanford, S. A., Eisenhardt, P. R., Elston, R., Spinrad, H., Stern, D., & Dey, A. 1999, *AJ*, 118, 76
- Stanford, S. A., et al. 2005, *ApJ*, 634, L129
- Stauffer, J. R., et al. 2007, in *American Institute of Physics Conference Series*, Vol. 943, The Science Opportunities of the Warm Spitzer Mission Workshop, ed. L. J. Storrie-Lombardi & N. A. Silbermann, 43
- Surace, J., Shupe, D. L., Fang, F., Lonsdale, C. J., & Gonzalez-Solares, E. 2005, *SSC website release*
- Warren, S. J., et al. 2007, *MNRAS*, 375, 213
- Werner, M. W., et al. 2004, *ApJS*, 154, 1
- White, S. D. M., et al. 2005, *A&A*, 444, 365
- Wilson, G., Muzzin, A., Lacy, M., & the FLS Team. 2005, *ArXiv Astrophysics e-prints (astro-ph/0503638)*
- Wilson, G., et al. 2006, *ArXiv Astrophysics e-prints (astro-ph/0604289)*
- Yee, H. K. C., Ellingson, E., & Carlberg, R. G. 1996, *ApJS*, 102, 269
- Yee, H. K. C., Gladders, M. D., Gilbank, D. G., Majumdar, S., Hoekstra, H., & Ellingson, E. 2007, in *Astronomical Society of the Pacific Conference Series*, Vol. 379, *Cosmic Frontiers*, ed. N. Metcalfe & T. Shanks, 103
- Yee, H. K. C., & López-Cruz, O. 1999, *AJ*, 117, 1985
- Zwicky, F., Herzog, E., & Wild, P. 1968, *Catalogue of galaxies and of clusters of galaxies (Pasadena: California Institute of Technology (CIT), 1961-1968)*

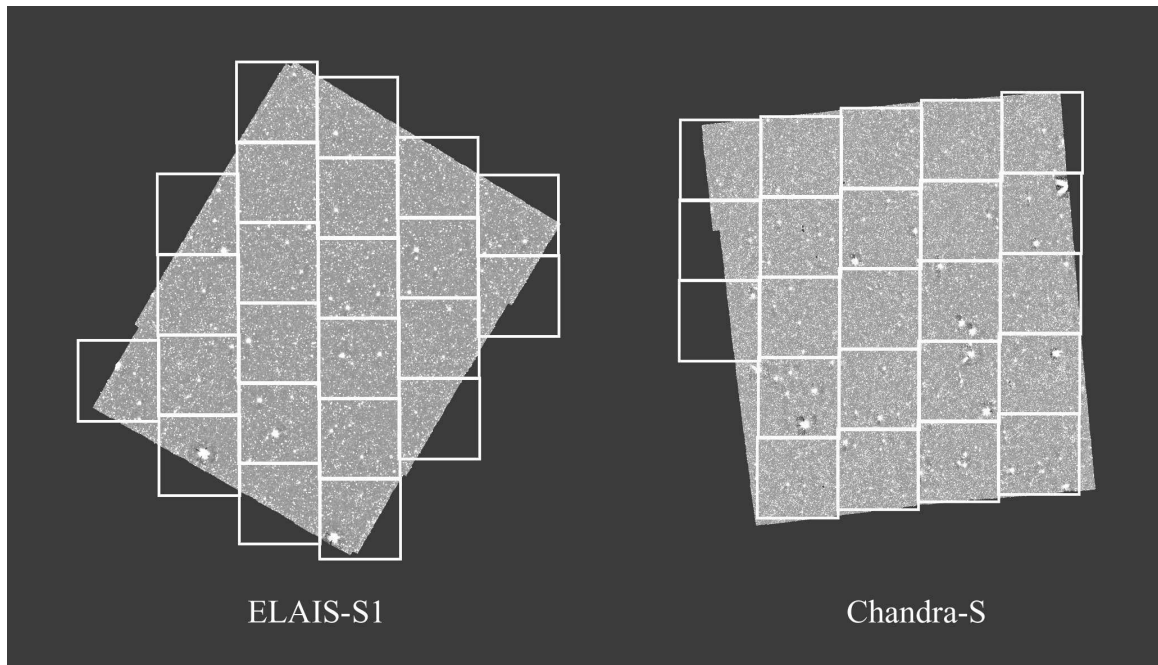


FIG. 1.— The SWIRE $3.6\mu\text{m}$ IRAC mosaics are shown in grayscale. The roll angle of the Spitzer Space Telescope on the date of observation determines the orientation of the IRAC observations. The white squares overlaid show the 46 CTIO MOSAICII pointings. There are 23 MOSAICII pointings each in the SWIRE 7.1 deg^2 ELAIS-S1 and 8.1 deg^2 Chandra-S fields.

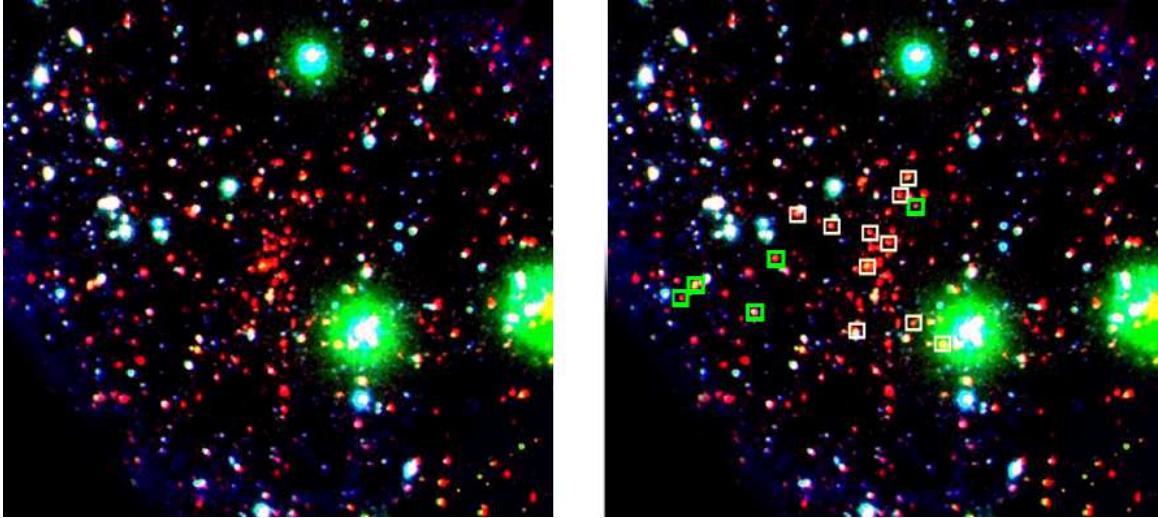


FIG. 2.— $r'z'[3.6]$ color composites of J003550-431224 are shown in both panels. The FOV is 1.5 Mpc at the cluster redshift. The white (green) boxes overlaid on the right panel show the 10 cluster members (5 foreground/background galaxies) with spectroscopically-confirmed redshifts from Gemini/GMOS-S (see Table 2).

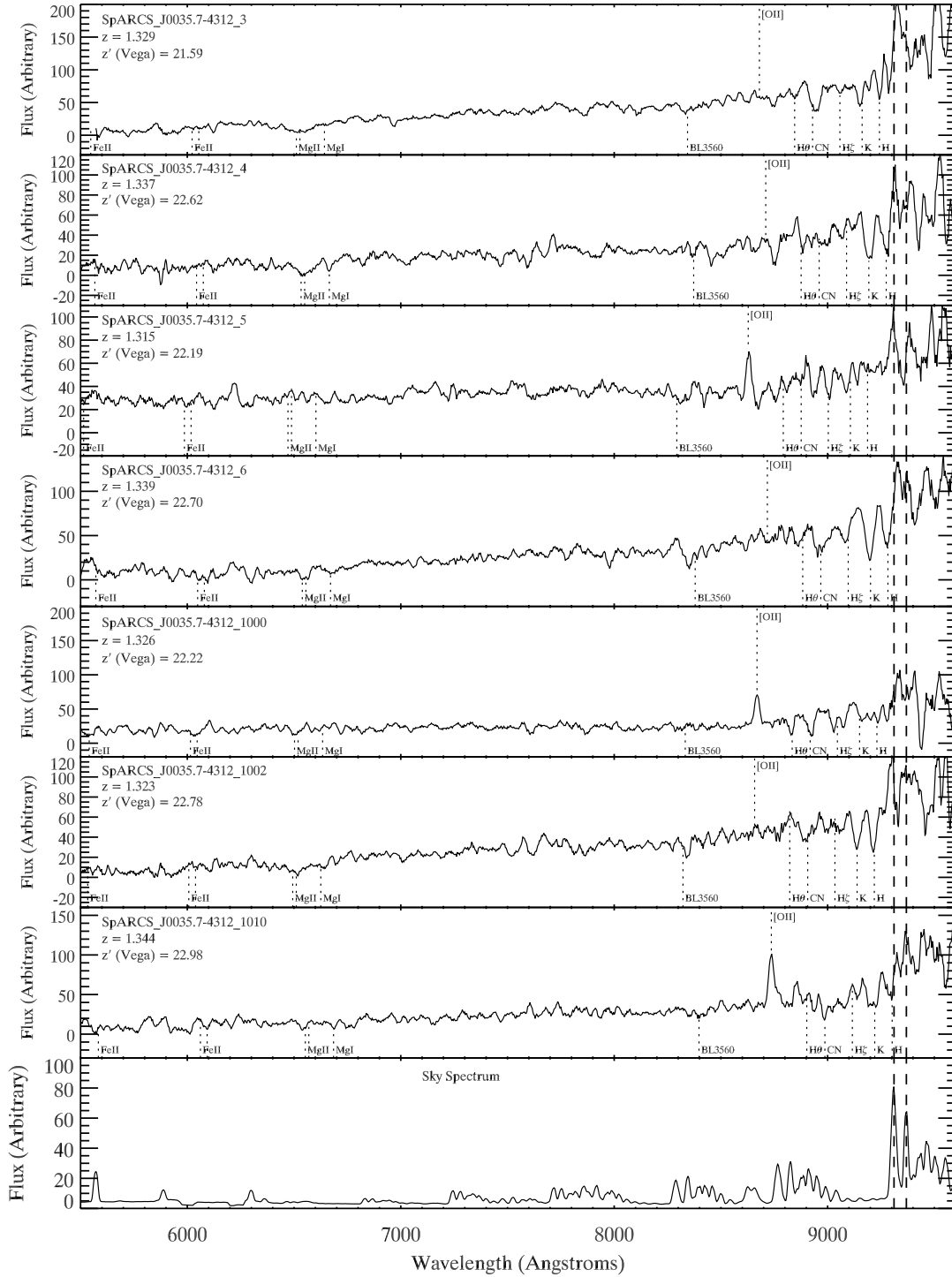


FIG. 3.— Spectra for a subsample of seven galaxies in cluster SpARCS J003550-431224 (see Table 2). The spectra have been smoothed with a 7-pixel (11\AA) boxcar. The identified spectral features are marked. The lowermost panel shows the typical sky spectrum.

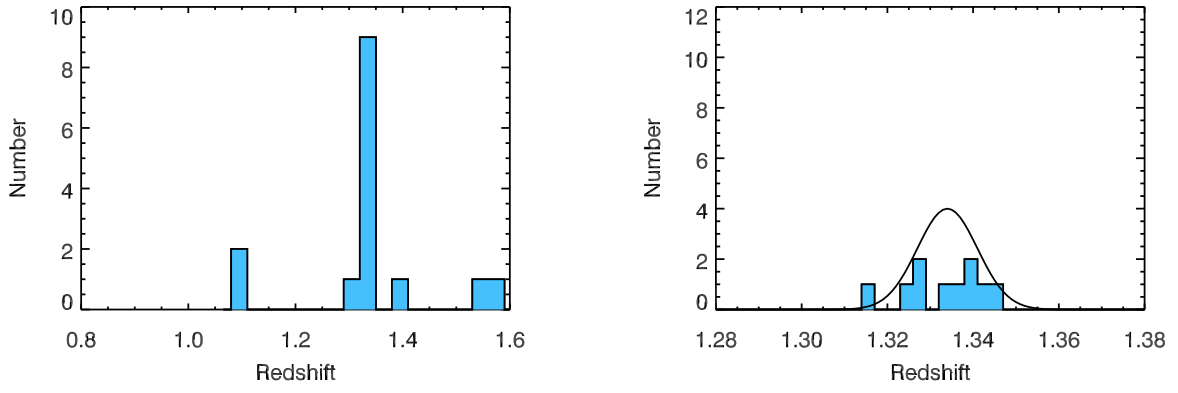


FIG. 4.— Histogram showing 15 galaxies with confirmed redshifts (left). Ten galaxies are confirmed as cluster members (right) and five are confirmed as foreground or background sources. See Table 2 for further details. A Gaussian with an r.m.s. of 1050 km s^{-1} (see § 5) has been overlaid

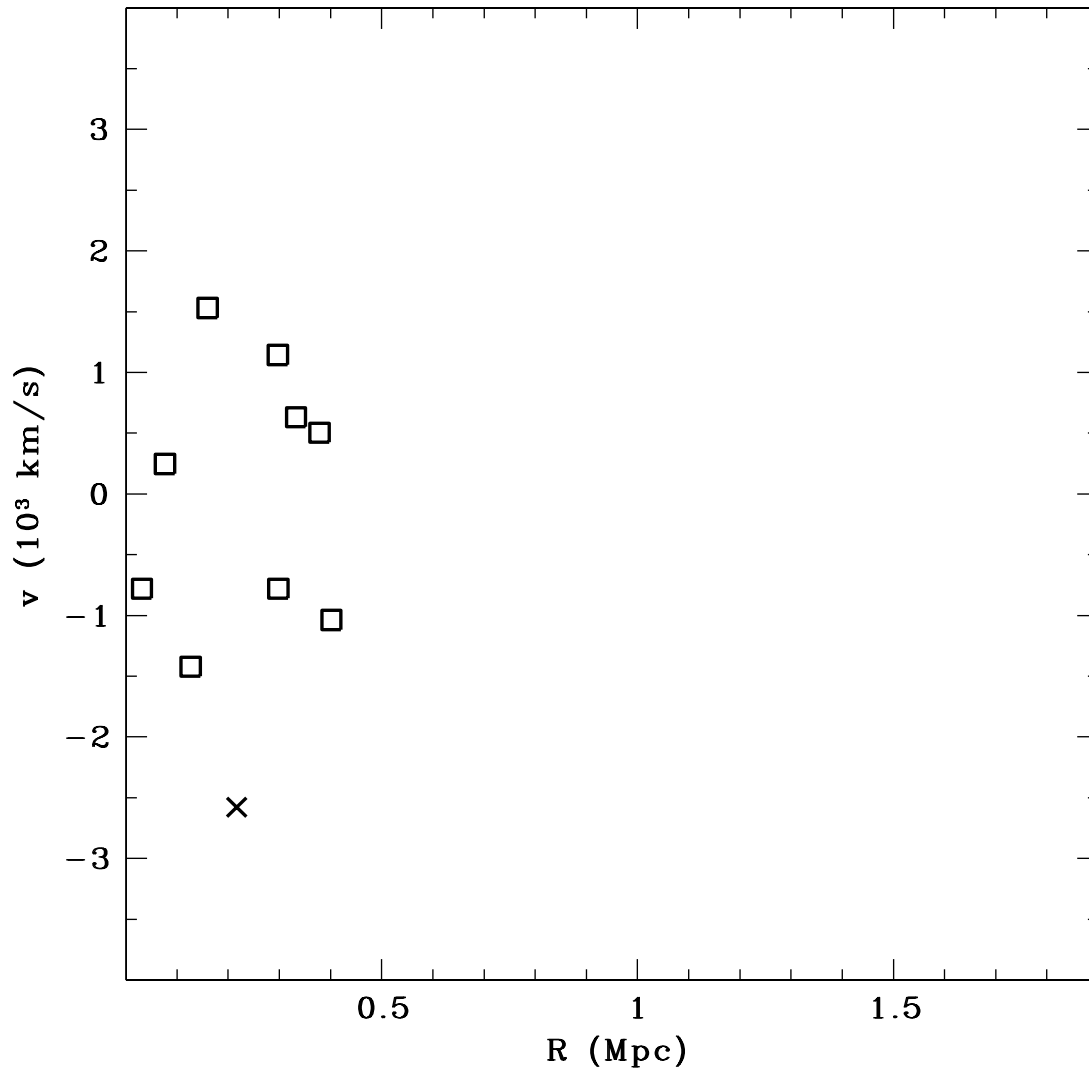


FIG. 5.— Galaxy velocities relative to the mean velocity, as a function of radius. The galaxy marked with an “x” (ID # 5 at $z = 1.315$ in Table 2) is more likely to a near-field object than a member of the cluster and was not used in the computation of the mean redshift or velocity dispersion.

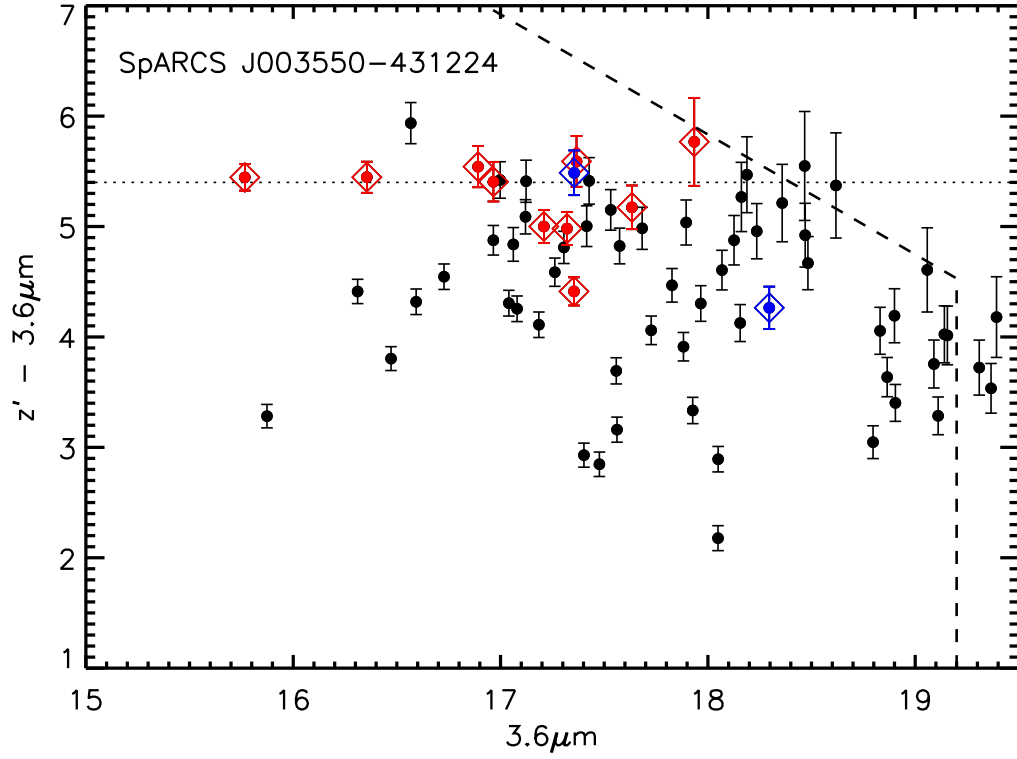


FIG. 6.— $z' - [3.6]$ versus $[3.6]$ color-magnitude diagram for SpARCS J003550-431224. The black circles are all the galaxies contained within a circle of radius 550 kpc ($65''$) at the cluster redshift. The red diamonds show the ten spectroscopically confirmed cluster members. The blue diamonds show the two (of the five) confirmed foreground/background galaxies which fall within the 550 kpc radius. The dotted line indicates the nominal red-sequence color for this cluster ($z' - [3.6] = 5.4$). See § 5 for a discussion.

TABLE 1
THE SPARCS FIELDS.

Field	R.A. J2000 (Deg.)	Decl. J2000 (Deg.)	SWIRE 3.6 μ m Area(deg ²)	SpARCS z' Area(deg ²)	Usable Area(deg ²)
ELAIS-S1	00:38:30	-44:00:00	7.1	8.3	6.5
XMM-LSS	02:21:20	-04:30:00	9.4	11.7	7.3
Chandra-S	03:32:00	-28:16:00	8.1	7.9	7.1
Lockman	10:45:00	+58:00:00	11.6	12.9	9.7
ELAIS-N1	16:11:00	+55:00:00	9.8	10.3	7.9
ELAIS-N2	16:36:48	+41:01:45	4.4	4.3	3.4
Total			50.4	55.4	41.9

TABLE 2
SPECTROSCOPIC REDSHIFTS IN THE
FIELD OF SPARCSJ0035.7-4312

ID	R.A. J2000 (Deg.)	Decl. J2000 (Deg.)	z' Mag Vega	z
Members				
3	0.597095	-43.20612	21.59	1.329
4	0.596806	-43.20263	22.62	1.337
5	0.598068	-43.19822	22.19	1.315
6	0.596565	-43.19285	22.70	1.339
1001	0.596076	-43.21811	22.22	1.327
1002	0.596473	-43.21479	23.69	1.329
1009	0.597075	-43.20102	22.78	1.324
1010	0.597606	-43.20000	22.28	1.347
1012	0.596664	-43.19551	22.98	1.344
3002	0.597252	-43.21589	21.81	1.340
Foreground/Background				
1	0.599490	-43.20939	22.33	1.100
1007	0.598371	-43.20495	22.84	1.394
2010	0.599674	-43.21098	22.98	1.104
3003	0.598673	-43.21307	21.62	1.550
4001	0.596434	-43.19699	22.68	1.581